Philosophical Magazine,
Vol. 85, No. 28, 1 October 2005, 3357–3378

Taylor & Francis
Taylor & Francis Group

On the rigid to floppy transitions in calcium silicate glasses from Raman scattering and cluster constraint analysis

M. MICOULAUT*†, M. MALKI‡§, P. SIMON‡
and A. CANIZARES‡

†Laboratoire de Physique Théorique des Liquides, Université Pierre et Marie Curie, Boite 121, 4, Place Jussieu, 75252 Paris Cedex 05, France
‡Centre de Recherche sur les Matériaux à Haute Température, CNRS, 1D, Avenue de la Recherche Scientifique 45071 Orléans Cedex 02 France
§Ecole Polytechnique de l'Université d'Orléans, 8 rue Léonard de Vinci, 45072 Orléans Cedex 02 France

(*Received 4 April 2005; in final form 21 April 2005*)

Calcium silicate glasses $x\mathrm{CaO}-(1-x)\mathrm{SiO_2}$ exhibit a threshold in Raman lineshapes which can be related, on the basis of Maxwell constraint counting, to the onset of network rigidity as the concentration of calcium oxide x is decreased. The present results are more deeply characterized by a size-increasing cluster approximation that allows to perform Maxwell mechanical constraint counting beyond the usual meanfield treatment. This permits to discuss under which structural conditions an elastic intermediate phase should be obtained in the future.

1. Introduction

Magmatic liquids are the principal agents of mass and heat transfer in the Earth and terrestrial planets and intensive research has been undertaken to understand the processes of mass or energy transfer with respect to melt or structural properties [1, 2]. Viscosity and thermal or electrical conductivity are indeed directly related to the structure of silicate melts which, furthermore, control the thermal behaviour of magmas and their formation or crystallization [3, 4].

In this context, calcium silicates of chemical formula $x\mathrm{CaO}-(1-x)\mathrm{SiO_2}$ have received little attention as compared to the corresponding alkaline systems so that much of their properties over the whole calcium glass formation range are still a subject of active research. Most studies have indeed focused on the $x=0.50$ molar concentration which corresponds to the crystalline wollastonite composition [5]. Several studies have stressed the special role played by the calcium atom which acts as a modifier in the silicate networks [6] and leads to a global increase of the

*Corresponding author. Email: mmi@lptl.jussieu.fr

Philosophical Magazine
ISSN 1478–6435 print/ISSN 1478–6443 online
http://www.tandf.co.uk/journals
DOI: 10.1080/14786430500157029

density from $2.75\,g\,cm^{-3}$ at $x=0.38$ to $2.97\,g\,cm^{-3}$ at $x=0.60$ pyrosilicate composition [7, 8]. Extensive studies have been performed to understand the miscibility limits in this system and in other alkaline earth silicates [9, 10].

A special attention has been devoted to the coordination number of the calcium atom using EXAFS [11] and X-ray spectroscopy [12]. More recently, Yannopoulos and co-workers have been studying inelastic light scattering of calcium silicates around the $x=0.50$ composition by polarized Raman spectroscopy [13]. The results with composition show a marked change in behaviour around 47% calcium. Specifically, intensity ratios of particular Raman lines as well as the boson peak frequency present a sharp jump at this concentration. On the other hand, a line at $606\,cm^{-1}$ shows an abrupt increase but there remains some uncertainty about its attribution to the so-called D_2 ring line [14]. However, the conclusion obviously suggests the presence of a transition that has not been characterized by the authors.

In this work, we show using Raman spectroscopy that a very particular elastic state is reached in the glass when the concentration of calcium x(CaO) equals 47%. This threshold is identified with a rigid to floppy transition from Maxwell mechanical constraint counting and suggests that elastic transition can take place in calcium silicate glasses as in chalcogenides [15, 16]. In the latter, the addition of cross-linking units such as germanium or silicon into a basic network made of twofolded chalcogenide atoms (sulphur, selenium) constrains the internal degrees of freedom of the network by increasing the number of bond-bending and bond-stretching forces that can lead to a very peculiar situation when the number of constraints per atom equals the number of degrees of freedom [17]. It has been identified by Thorpe from numerical simulations on amorphous silicon as being a floppy to rigid transition characterized by the vanishing of the number of normal (floppy) modes of the dynamical matrix [18, 19]. The glass transition temperature of such systems undergoing a rigid to floppy transition is also substantially affected [20].

More recently, Raman scattering results [21] and temperature modulated calorimetry [22] on very different glassy selenides have shown that there were in fact two transitions. These observations have been also found from numerical simulations [23] and cluster calculations [24]. Both predict that when a network is progressively stiffened, the first transition takes place with the onset of rigidity when the number of constraints per atom equals the number of degrees of freedom. The second transition is a stress transition which corresponds to the point beyond which stress (hyperstatic regions) in the network cannot be avoided any more with increasing cross-linking units. Percolation of rigidity and percolation of stress define the boundaries of an intermediate phase which is rigid but stress-free. Elasticity with applied pressure has been studied in this kind of systems, which provides a measure of the local stress and suggests that one has an isostatically rigid backbone inside the intermediate phase [25]. Isostaticity also accounts for the non-aging behaviour of glasses [26] observed in this same composition range.

These new concepts or rigidity and rigidity transitions have been successfully applied to the study of network chalcogenide glasses. As the ingredients used in the onset of rigidity and the origin of the intermediate phase are quite generic, one may expect that these show up (i) in other non-chalcogenide glass systems and (ii) in other fields. For the latter issue, it has been shown that there are some obvious links between rigidity theory and computational phase transitions [27], high T_c

superconductors [28] or protein folding [29]. Extensions from chalcogenide to e.g. oxide glasses have been reported only very recently. It has been indeed shown from molecular dynamics simulation and experiment [30] that the same floppy to rigid transitions could be found in oxide glasses under pressure with a pressure window found in both densified GeO_2 and SiO_2 that bears striking similarities with the measured intermediate phase in chalcogenides. Furthermore, experiments from calorimetry and Brillouin scattering [31] applied on sodium silicates reproduce exactly the salient features of onset of rigidity and stress. Understanding to what extent the methods used with success for the chalcogenides can be applied to oxide glasses is therefore not only of fundamental interest but also of attractive perspective for applied purposes [32]. Recently, the signature of a rigid to floppy transition has been detected in this system from electrical conductivity measurements [33] that show percolation of the mobility. With these new reported examples, the generic effect of rigidity on various physical quantities in any kind of networks is clearly emphasized. The study of a different oxide glass system such as calcium silicates, lies clearly in this prospect.

We first display the results of the Raman analysis and the deconvolution of the spectra which show a marked change in behaviour for some modes at $x = 0.47$. Next, we apply on this system mean-field Maxwell mechanical constraint counting that permits to compute the concentration x_c at which the fraction of zero frequency (floppy) modes vanishes [18]. We improve the approach in section 4 by analyzing the present system with size-increasing cluster approximations (SICA) that infer the effect of medium-range order on the nature and the location of the transition, which is found to be in agreement with experimental findings. Finally, we show which conditions in terms of medium range order have to be satisfied in order to obtain an intermediate self-organized phase [34] that is bounded by a rigidity and a stress transition [23], in close correspondence with the chalcogen analog.

2. Experimental results

2.1. *Sample preparation*

The samples were prepared by mixing pre-dried SiO_2 (99.99%) and $CaCO_3$ (99.95%) powders in the correct proportions. For each sample, the mixture was melted in a platinum crucible at 1650°C for 2 h, and quenched by placing the bottom of the crucible in cold water. The samples were then annealed at a temperature around 760°C for 5 h and cooled slowly to room temperature. The glasses were transparent and free of crystallization as confirmed by the absence of Bragg peaks in XRD spectra. Chemical microanalysis using the energy-dispersive X-ray (EDX) performed on optically polished glasses showed a very low departure (less than 0.4 mol of Ca) between the theoretical and the real composition for all the studied samples. The glass transition temperatures were determined with a differential scanning calorimeter Setaram DSC-1600 at a heating rate 10°C/min. These values (see table 1) are slightly larger than those reported by Shelby [35] using the dilatometric technique, but they exhibit the same global trend. The glass-forming region of the calcium silicate system is rather narrow [typically 0.40–0.55 CaO] and explains the concentration range investigated in the present paper [36].

Table 1. Glass transition temperatures of the $(1-x)SiO_2 - xCaO$ system.

Concentration x	42	44	47	50	53
T_g [°C]	769	769	770	781	795

2.2. *Raman scattering*

Raman spectra were obtained on a Jobin-Yvon T64000 spectrometer with CCD detection and BX40 Olympus microscope (objective $\times 100$). The excitation wavelength was the 514.532 nm argon line of a Coherent Innova 70 Spectrum laser. The power was typically 300 mW at the laser output (20 mW on the sample). The low-frequency part range ($<500\,cm^{-1}$) was obtained in triple substractive mode (gratings 1800 gr/mm). For the high frequency part (above $300\,cm^{-1}$), the spectrometer was in simple monochromator configuration with Notch filter (grating 600 gr/mm). This allows a sufficient recovering spectral range for merging the spectra. All the data on the different compositions were collected in exactly the same conditions, one following each other, in order to be consistent throughout the series in any variation between subsequent spectra.

2.3. *Peak deconvolution*

The experimental spectra were first corrected for first-order Bose–Einstein factor, and also for scattering law ($I \simeq \nu^4$). The latter (a second-order correction compared to Bose–Einstein factor) is not of primary importance but is theoretically needed to extract the Raman susceptibility, which is the relevant physical quantity that can be used to extract information on dynamics. The Bose–Einstein reduction does not include the prefactor $1/\omega$ generally used for describing the low-frequency part of Raman spectra in glasses [37], according to the Shuker–Gammon formalism [38]. Examination of the bare spectra shows that the main variations upon increasing Ca content from 0.42 to 0.53 lie at wavenumbers above $300\,cm^{-1}$ and thus justify to focus attention on this spectral range. After this, the spectra were reconstructed with the FOCUS software [39], by using a log-normal law for the boson peak at low frequencies, and gaussian shapes for higher frequency ones. The low-frequency (boson peak) part was fitted to insure a correct description of the mid-frequency range, due to its long tail, but is clearly beyond the scope of the present paper. Moreover, recent hyperRaman measurements in silica tend to show that the boson peak responsible for the excess density of states is directly observed in hyperRaman and inelastic X-ray scattering, meaning that the low-frequency Raman component implies other degrees of freedom and is then much more complicated to interpret [40]. For higher frequency modes, gaussian shapes gave a better reconstruction of the spectra than lorentzian or damped harmonic oscillator ones.

3. Discussion

3.1. *Spectra description*

Figure 1 displays the experimental Raman data for the six CaO concentrations 0.42 to 0.53. Figure 2 exhibits the typical agreement between experimental and fitted

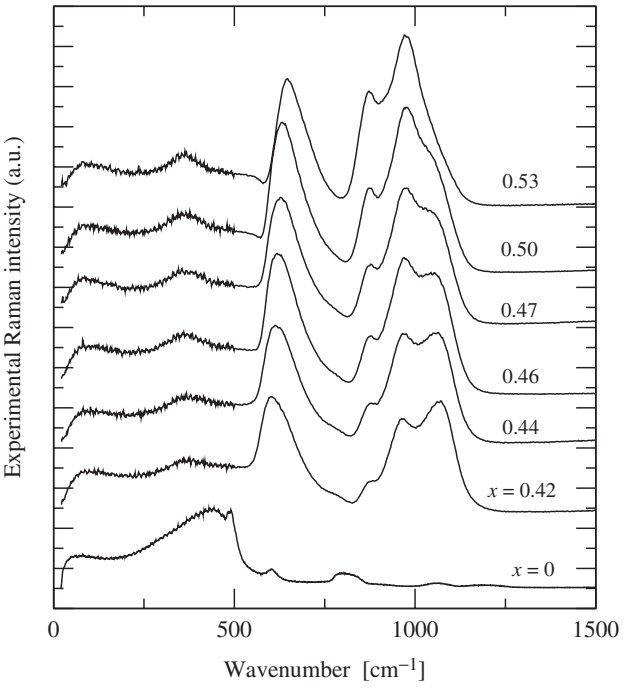

Figure 1. Raman lineshapes for six CaO concentrations. The low wavenumber range was acquired in triple substractive mode (see text) which explains the higher noisy level. The spectrum of silica at the bottom of the figure is displayed for comparison.

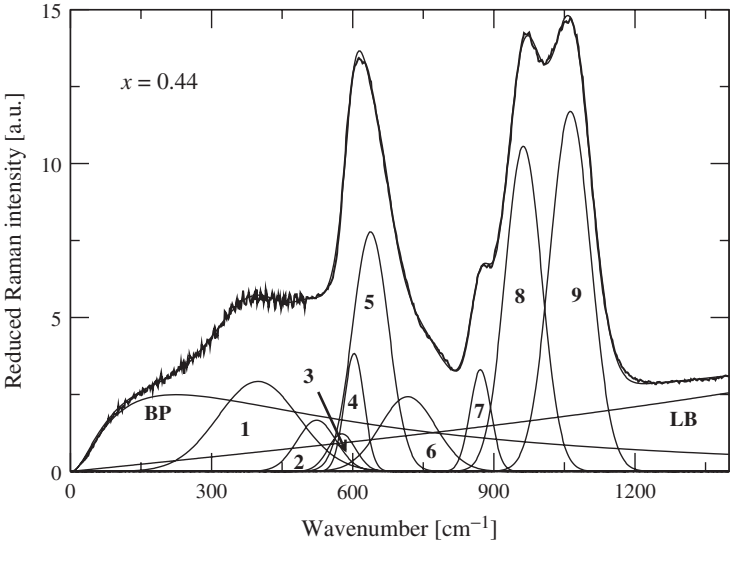

Figure 2. Fits of the Raman spectra of the $x = 0.44$ sample. The numbers (1–9) correspond to the various gaussian deconvolutions of the spectra (see text for details). BP is the boson peak and LB the luminescence background.

spectra (Bose–Einstein and scattering corrected). Results of the fitting procedure are displayed in the different panels of figures 3 and 4 (line wavenumbers, linewidths, and integrated intensity). The whole concentration range was described with 9 modes (plus the boson peak) : 3 modes in the range below 550 cm^{-1}, 3 modes to describe the sharp and asymmetric peak near 600 cm^{-1}, and 3 modes for the higher-frequency group around 1000 cm^{-1}. A broad luminescence background was needed to describe the intensity increase up to high relative frequencies, a feature that may be related with the presence of 3d impurities in the Ca precursor.

The 1000 cm^{-1} group is sometimes described by four components or more. We consider that as only three bumps are unambiguously visible in the spectra, the lowest number of components giving satisfactory reconstruction of the experimental data is the best possible choice. The four components needed by Kalampounias *et al.* [13] look obviously necessary on their data for $x > 0.55$ and $x < 0.40$, but not in the range investigated here.

Modes 2 and 3 are somewhat weak and then are rather inaccurate (at least compared to other ones) as their possible parameter variation in the Ca range is hindered by experimental uncertainty. Mode 1 is discussed below. The accuracy is better for modes 4 and 5. Both wavenumbers increase monotonously upon increasing Ca concentration (see figure 3). Their intensities show a transfer from 5 to 4 near 47% Ca. The linewidth of mode 4 shows a smooth increase whereas that of mode 5 abruptly, narrows at compositions greater than 50% CaO. The greater effects concern the higher frequency modes, 6, 7, 8, and 9. One can first consider the latter three modes, clearly connected in one broad band. This assignment slightly differs from [13], where mode 7 is assigned to Q^0 species, and from Frantz and Mysen [41] where Q^3 corresponds to a weaker mode and mode 8 is assigned to Si–O stretching vibrations. The superscript n in Q^n denotes the number of bridging oxygens (not connected to Ca) on a $SiO_{4/2}$ tetrahedra. According to Zotov [42], mode 9 can be assigned to Q^3 species, mode 8 to Q^2 and mode 7 to Q^1. The wavenumbers for modes 7 and 8 are practically constant. It is not the case of their intensities, which show a continuous increase for modes 7 and 8, whereas for mode 9 is rather constant up to 47% Ca, and decreases rapidly after. The wavenumber of mode 9 displays a decrease up to around 47% Ca, and then a slight increase. This effect is small but clearly large than experimental error. One can note that the sum of intensities of modes 8 and 9 is roughly constant above this value 47% Ca (figure 4). The linewidths of modes 7 and 8 increase slightly, whereas that of mode 9 is constant up to 47% CaO, and shortens after. From the foregoing, one can conclude that the increase of CaO affects the glass structure in two ways: first, a continuous increase of the number of Q^2 and Q^1 species to equilibrate the higher number of cations, and second a sharp transfer from Q^3 species to Q^2 ones upon increasing Ca content above 47%. Then the remaining Q^3 are more decoupled of the network, as shown by their lower linewidth.

Mode 6 is the most affected by the modification of Ca content as shown in figure 4. Its frequency is hugely increased (more than 50 cm^{-1}, which is considerable), the width of the line is decreased by more than a factor 2, between 42 and 48% Calcium Oxide, and its integrated intensity falls down by one order of magnitude in the same concentration range. When comparing with [13] where the 600 cm^{-1} asymmetric component is described only by one line, the present work shows that the anomaly around $x(CaO) = 47\%$ is only due to mode 6, the other

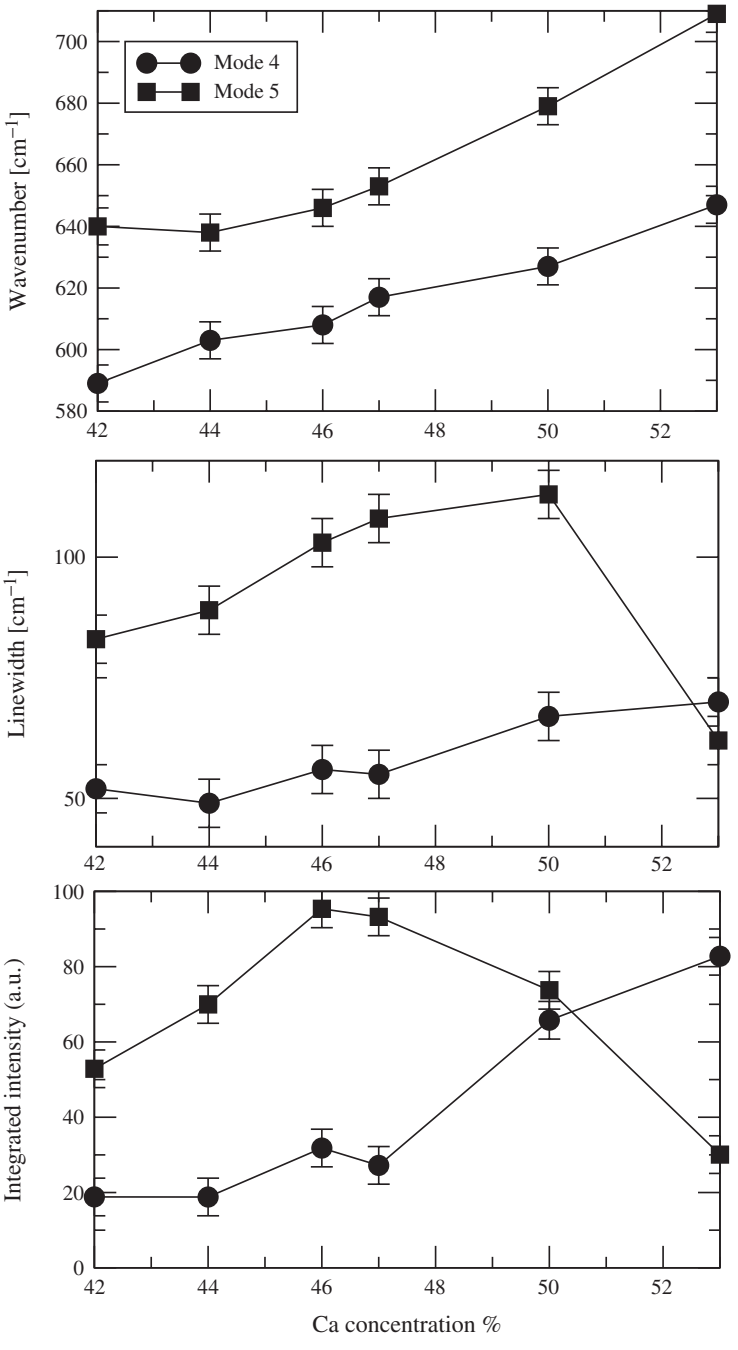

Figure 3. Composition behaviour in wavenumber, linewidth, and relative integrated intensity for the lines 4 and 5 of the Raman spectra in the $(1-x)SiO_2-xCaO$ system. There are no scale factors between the integrated intensities.

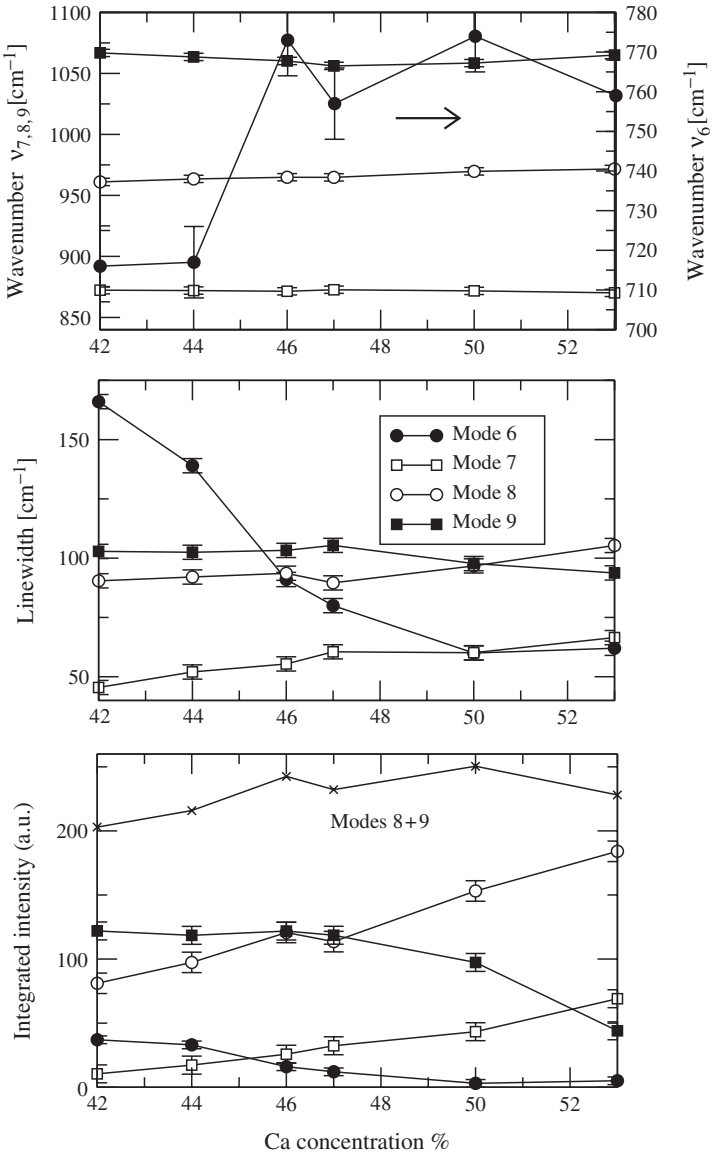

Figure 4. Compositional behaviour in wavenumber, linewidth, and relative integrated intensity for different lines (6–9) of the Raman spectra in the $(1-x)SiO_2 - xCaO$ system. The error bars are of the size of the symbols except for modes 6 and 9 wavenumbers.

modes 4 and 5 overlapping this component evolve monotonously in this composition range. This mode 6 cannot then be assigned to Q^0 species as the corresponding intensity must increase upon enriching Ca content. It is more plausibly connected with Si–O–Si motions. The intensity dependence, which is more rapid than for mode 9, would lead to think that mode 6 could correspond to Si–O–Si vibrations of $Q^3 - Q^3$ species.

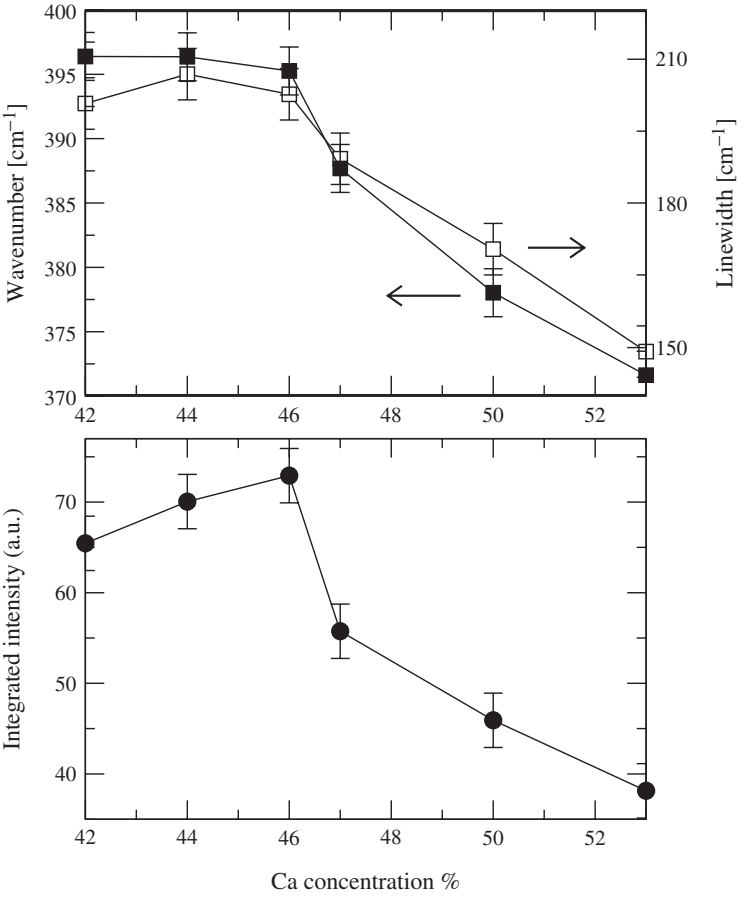

Figure 5. Compositional behaviour in relative wavenumber, linewidth and relative integrated intensity of the mode 1 line lying at 392 cm^{-1} for 42% Ca.

Mode 1 displays two specific features around 46–47% Ca. Its frequency exhibits a noticeable downshift (20 cm^{-1}), the width decreases by 30%, and the integrated intensity falls down by a factor two (figure 5). Even if this mode is broader than the preceding ones, these parameter evolutions are sufficiently large to be unambiguous. This frequency downshift and line narrowing upon increasing Ca content is different from high-frequency modes (6, 9). This softening and narrowing is an uncommon behaviour and can be qualitatively explained only by a significant change of eigenvectors. The low frequency of this mode implies some Ca vibrations. These vibrations would then be decoupled, and softer, above ca. 46%, that can be attributed to floppy regions in the glass.

3.2. *Raman threshold and rigid to floppy transitions*

The results on the behaviour of some Raman modes with concentration closely parallel that found in chalcogenides [43]. The frequency increase exhibited by

modes 6 and 9 above 47% calcium can indeed be discussed in the context of rigid to floppy transitions. In fact, these modes look to harden just when the network becomes softer. This apparent contradiction can be explained by a non-uniform distribution of stress: in the stressed rigid range close to our observed threshold at $x = 0.47$, the network is mainly hardened by interconnected Q^3 species. Upon undergoing a rigidity transition, these links should become much less numerous, leading to a network which is dominated by Q^2 connections. The remaining Q^3 domains will then be smaller and consequently more homogeneous, this is evidenced by the noticeable line narrowing which occurs. The distribution of Q^3 force constants is less important, leading to a linewidth closer to a lorentzian one. These Q^3 islands lie then in the holes of the Q^2 network. The increase of mode 9 (Q^3) line wavenumber can then be easily explained by partial decoupling of Q^3 vibrations inside islands from the Q^2 network, leading to a wavenumber closer to that of an alone Q^3 tetrahedron. In the floppy range at high CaO concentration, the structure should be a network of Q^2 elements, separated by small 'harder' islands. The narrowing exhibited by mode 5 above 50% can also be interpreted in the same way.

We finally note that only selected Raman modes are active in the detection of the rigid to floppy transition. This is obvious for the modes 1 and 6 and also for mode 5. From the analysis displayed above, it appears that the onset of rigidity affects rather intertetrahedral motions (mode 6, Si–O–Si motions, see aforesaid) than e.g. intratetrahedral symmetric stretching vibrations (modes 7–9). Nevertheless, the latter modes can be sensitive to the transition because of the coherent motion between tetrahedra. It contrasts with binary chalcogenides where the majority of the Raman modes [43] were displaying some characteristic behaviour at the thresholds. We stress, however, that the structure of the latter system is much more simpler than the present silicates.

4. Analysis from constraint theory

Maxwell constraints counting appears to be useful to understand the present results as the calcium silicate network can be described by a molecular system constrained by bond-stretching and bond-bending (angular) forces.

4.1. *Maxwell global constraint counting*

We consider the $CaO–SiO_2$ system as a network of N atoms composed of n_r atoms that are r-fold coordinated. Enumeration of mechanical constraints [17–19] associated with bond-stretching (radial) forces leads to $n_c^\alpha = r/2$, while the number of bond-bending (angular) constraints is $n_c^\beta = (2r - 3)$. The average number of floppy modes per atom F/N in this three-dimensional network is given by [19]:

$$f = \frac{F}{N} = n_d - n_c = 3 - \frac{1}{N}\sum_{r\geq 2} n_r\left(\frac{5r}{2} - 3\right) \tag{1}$$

where n_d is the dimension of the network and $n_c = n_c^{\alpha} + n_c^{\beta}$. Applied to the system of interest leads to:

$$f = \frac{F}{N} = 3 - \frac{11 - 7x}{3 - x} \tag{2}$$

The latter equation holds if one assumes that silicon is fourfold, calcium and oxygen are twofold coordinated [44]. The constraint counting applied in the present system cannot be applied down to $x = 0$ (Silica) as the latter has broken bond-bending constraints [45] due to the partial ionic character of Si–O bonds as shown from the broad angular Si–O–Si distribution. Specific counting has therefore to be accomplished for silica that has a certain number of floppy modes and is found to be floppy [46]. With addition of alkali oxide, the angular distribution becomes sharper [47] thus suggesting that at some point the bond-bending constraints are restored.

As one can see, the number of floppy modes vanishes when the network attains the critical concentration $x = x_c = 0.50$ which is in close agreement with the thresholds observed from our Raman results. The calcium coordination number of two is used to obtain equation (2) deserves some supplementary comments because EXAFS studies [11] and computer simulations [48] have suggested that the number of nearest neighbours of the calcium could be different from the formal valence of 2 and would rather be of the order of 6. On the other hand, the Debye–Waller factors for this system or related alkaline earth silicates [11] clearly show that the oxygen atoms around a calcium atom were not all equivalent, thus confirming the picture drawn by Kerner and Phillips [44] on resonating bonding constraints that lead to an effective number of constraints for the calcium of 2. Finally, we mention that the use of an effective number of constraints in related sodium silicates [31] permits to recover from experiment the mean-field threshold at correct critical concentration of sodium, although the number of oxygen neighbours in the vicinity of a sodium atom is usually found to be larger [49] than one.

Equation (2) defines a mean-field transition in which the number of mechanical constraints is computed from the macroscopic concentration x. Obviously, this elastic transition may be attained at $x < x_c$ provided that some macroscopic floppy subregions can emerge with the addition of alkaline earth oxide. On the other hand, it has been recently shown [23, 24] that the underlying nature of the floppy to rigid transition was more subtle and could contain under certain circumstances [34] two transitions instead of the single one predicted by mean-field constraint counting. In this context, stress will not spread randomly over the whole network as initially believed but will accumulate in underconstrained subregions leading to the occurrence of an intermediate elastic phase that is found to be stress-free. The detection of this intermediate phase has been mostly accomplished from calorimetric probes using temperature modulated differential scanning calorimetry (MDSC) [50]. Here, a sinusoidal variation is added on the usual linear DSC ramp and permits to decompose the total heat flow into a reversing part that tracks the initial modulation and a residue. The latter is found to vanish in the intermediate phase [34].

4.2. *Cluster construction*

Size-increasing cluster approximations (SICA) appear to be a useful tool to describe the elastic nature of the network backbone (floppy, intermediate, stressed rigid) and permits to take into account medium-range order effects that may, or may not, serve as ingredient for the presence of an intermediate phase. Furthermore, SICA start from the mean-field description as basic level and take into account non-random structural elements and their related mechanical constraints in a systematic fashion. This method was first introduced to study the formation of fullerenes [51] or Penrose tilings in quasicrystals [52] and was then applied to quantify the boroxol ring statistics in amorphous B_2O_3 [53]. Recently, SICA has been used in the context of floppy to rigid transitions [24] in an archetypal chalcogenide network (Ge_xSe_{1-x}) and has led to the definition of a stress-free intermediate phase that depends substantially on the fraction of small rings in the structure.

The basic level ($l=1$) of the SICA construction corresponds to the mean-field approximation, having as elements structural species that depend directly on the macroscopic concentration. The construction permits to generate clusters at step $l=2$ sharing all possible combination of the basic ($l=1$) elements, clusters at step $l=3$ having three ($l=1$) units, etc. The probabilities of the clusters are computed within the Canonical Ensemble having energy levels E_n related to bond creation between the basic level molecules. The construction is, furthermore, supposed to be performed at the formation of the network when T equals to fictive temperature $T_{fictive}$ which is defined by the intersection of the extrapolated supercooled liquid and glass curves [54]. Mathematically, these probabilities will involve statistical weights (or degeneracies $g(E_n)$ of a corresponding energy level), which correspond to the number of equivalent ways to connect two ($l=1$) basic units, and a Boltzmann factor [54] of the form $e_n=\exp[-E_n/T_f]$.

We have used as basic units the CaO molecule and a $SiO_{4/2}$ tetrahedron, having for respective probabilities the macroscopic concentration x and $(1-x)$. The energy levels are defined from the consideration of all possible connections at the step $l=2$ and permit to distinguish the mechanical nature of the underlying clusters (floppy, isostatic, stressed). The creation of a chain-like Ca_2O_2 floppy structure ($n_c<3$) is related to an energy gain of E_f while the creation of a CaO connected to a silicon tetrahadron (an isostatically rigid $CaSiO_3$ cluster, $n_c=3$) is associated with an energy E_i. Finally, the basic network, formerly represented by two connected $SiO_{4/2}$ tetrahedra (a stressed rigid Si_2O_4 cluster, $n_c>3$), corresponds to an energy gain of E_s. At step $l=2$, three different clusters can be obtained (see figure 6) and their probabilities are given next. We mention that edge-sharing $SiO_{4/2}$ tetrahedra have been excluded from the construction as they have no experimental evidence at all in silicates [55]. The probabilities at step $l=2$ are:

$$p_1=\frac{16(1-x)^2e_s}{4x^2e_f+16x(1-x)e_i+16(1-x)^2e_s} \tag{3}$$

$$p_2=\frac{16x(1-x)e_i}{4x^2e_f+16x(1-x)e_i+16(1-x)^2e_s} \tag{4}$$

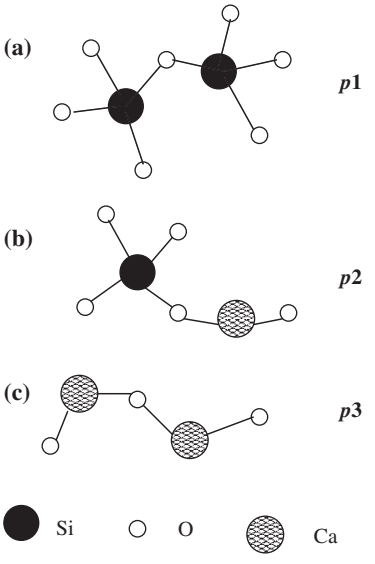

Figure 6. The different clusters obtained at SICA step $l=2$. (a) A fragment of the silica network with $g(E_s)=16$, (b) a wollastonite-like cluster $CaSiO_3$ with $g(E_i)=16$, and (c) a calcium-rich cluster with $g(E_f)=4$.

$$p_3 = \frac{4x^2 e_f}{4x^2 e_f + 16x(1-x)e_i + 16(1-x)^2 e_s} \tag{5}$$

out of which the ($l=2$) concentration of calcium atoms can be computed

$$x^{(2)} = \frac{p_2 + 2p_1}{4 - p_2 - 2p_1} \tag{6}$$

Due to the initial choice of the basic units, the energy E_i will mostly determine the probability of isostatic clusters since the related Boltzmann factor e_i is involved in the probability (4) of creating the isostatic $CaSiO_3$ cluster (a CaO–$SiO_{4/2}$ bonding). In the case where $E_i \ll E_f$, E_s, the bonding of the network construction will be mainly achieved by isostatic clusters.

For large steps ($l>2$), one has to take care of possible isomers produced by two distinct clusters at the lower level. The cluster displayed in figure 7a can be, for example, produced either by connecting two $SiO_{4/2}$ tetrahedra onto a $CaSiO_3$ ($l=2$) cluster or by adding CaO and $SiO_{4/2}$ onto a Si_2O_4 ($l=2$) cluster. The statistical weight $g(E_n)$ of such isomers will be, of course, larger than the one of low connected clusters having a single pathway of production.

As seen from equations (3)–(5), the cluster probabilities will depend only on two energy parameters (i.e. the factors e_s/e_i and e_f/e_i) and the problem can still be reduced by using a charge conservation law [56] for the calcium atom applied on the population of clusters of size l.

$$x^{(l)} = x \tag{7}$$

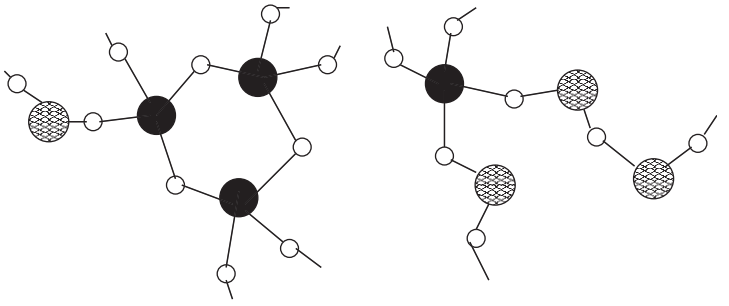

Figure 7. Clusters generated at SICA step $l=4$. (a) a 3-membered ring at low Ca concentration. (b) A high Ca structure.

The x-dependence of either e_s/e_i or e_f/e_i means that either the fictive temperature T_f or the energies E_n depend [54] on x but here only the $e_n(x)/e_i(x)$ dependence is relevant for the analysis.

In order to obtain some clusters having significant medium range order (figure 7b), the SICA construction has been realized up to the step $l=4$.

4.3. *Maxwell cluster constraint counting*

Next, one can apply on the generated set of clusters Maxwell constraint counting by enumeration of bond-bending and bond-stretching constraints and calculation of the corresponding expressions of n_c^{α} and n_c^{β}. Of particular importance are the structures containing a ring having less than six atoms (see figure 7a), because one has to remove some extra constraints [18].

For each step l, the total number of constraints $n_c^{(l)}$ can be computed as:

$$n_c^{(l)} = \frac{\sum_{i=1}^{\mathcal{N}_l} n_{c(i)} p_i}{\sum_{i=1}^{\mathcal{N}_l} N_i p_i} \tag{8}$$

where $\mathcal{N}_l$ is the total number of clusters of size l and $n_{c(i)}$ and N_i are respectively the number of constraints and the number of atoms of the cluster of size l with probability p_i. Applied to the set of clusters at step $l=2$, one obtains for example:

$$n_c^{(2)} = \frac{22p_1 + 15p_2 + 4p_3}{6p_1 + 5p_2 + 2p_3} \tag{9}$$

We have determined either e_s/e_i or e_f/e_i as a function of concentration, by solving the charge conservation law (7). With these factors depending on the concentration x, it is possible to compute the cluster probabilities p_i of given step l as a function of composition and finally obtain the composition x_c where the number of floppy modes $f_l = 3 - n_c^{(l)}$ vanishes. The statistics of the Q^n species with Ca concentration can also be computed as discussed next.

5. Results

5.1. *Structural properties and speciation*

In this section, we consider the solutions of the SICA construction in terms of structure. One principal objective of the present investigation is first to compare the model results with some experimental data on calcium silicate glasses such as the relative abundances and mixing properties of the structural units with respect to the concentration.

Figures 8 and 9 represent the distribution of Q^n units computed from SICA at step $l=4$, respectively as a function of Ca concentration and as a function of the relative abundance of non-bridging oxygens NBO/T that is defined by:

$$\sum_k n_k x(Q^k) = \frac{NBO}{T} \tag{10}$$

where n_k is the fraction of non-bridging oxygens per $SiO_{4/2}$ tetrahedra and $x(Q^k)$ is the concentration of Q^k species. The quantity defined by equation (10) is commonly used to quantify network depolymerization with non-bridging oxygens [57].

As one can see, the probability of findings a Q^4 unit decreases smoothly with the addition of calcium whereas the emergence of $Si_2O_5^{2-}(Q^2)$ and $SiO_3^{2-}(Q^3)$ groupings is noticeable. One can, furthermore, notice the crossover of the abundance of Q^2

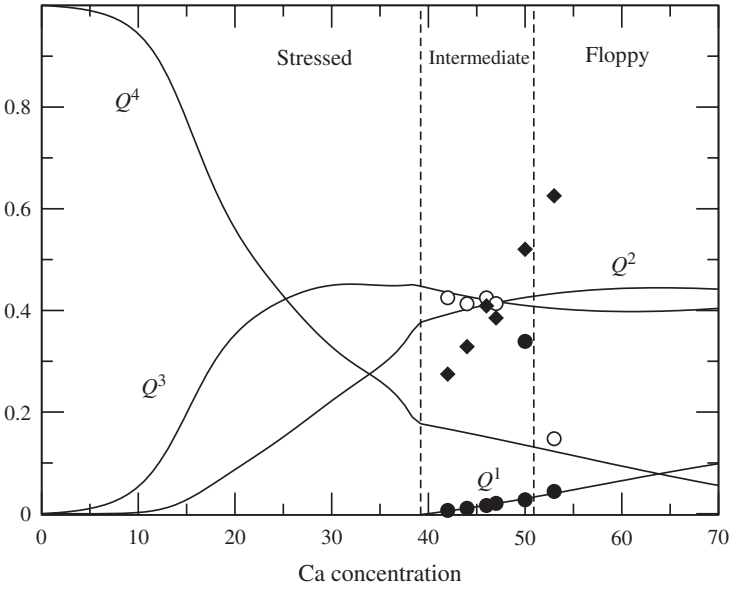

Figure 8. Q^n distribution in $(1-x)SiO_2 - xCaO$ as a function of the calcium concentration, computed at SICA step $l=4$. The vertical broken lines show the boundaries of the intermediate phase (see base line). The symbols are the results obtained from the Raman modes (see text for details).

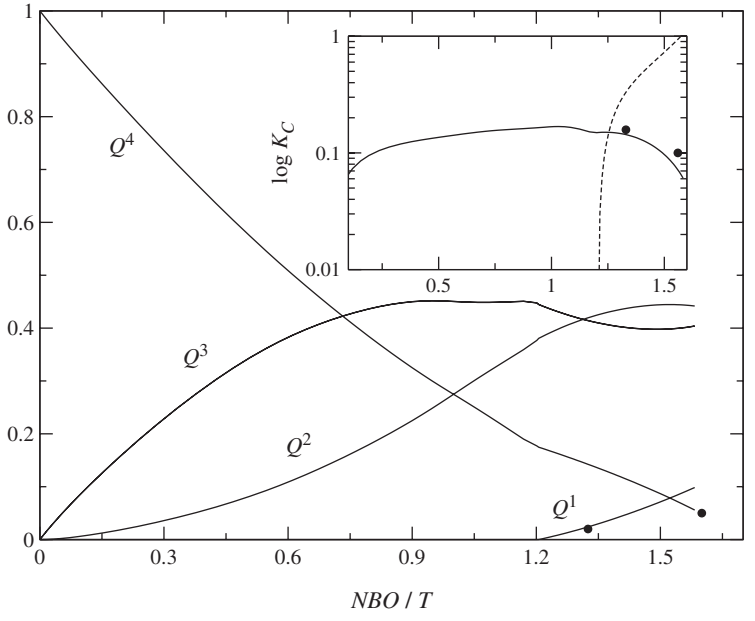

Figure 9. Q^n distribution in $(1-x)SiO_2 - xCaO$ as a function of NBO/T, computed at SICA step $l=4$. The insert shows the calculated equilibrium constant K_{C1} (solid line) and K_{C2} (broken line) as a function of NBO/T. See text for details. Data points are taken from Frantz and Mysen [31].

and Q^3 at the concentration $x=0.47$, a behaviour that has also been observed from the integrated intensity of modes 8 and 9 in the Raman spectra.

The general evolutions of populations of Q^n species look somewhat comparable, particularly for the Q^1 ones. To compare the results from SICA with those from the Raman spectra analysis, two aspects must be considered. First, the scattering cross sections are not identical for each Q^n species, and to make a comparison valuable, we have renormalized the Raman results of figure 8 to the SICA calculated ones at $x=0.47$. Second, the meaning of Q^n intensities are not exactly the same ones in the model (which gives the Q^n population in terms of a probability) and in Raman scattering. In the latter, the so called 'Q^n-line' intensity varies as the Q^n number but may not be exactly proportional to the Q^n number. For Q^2, Q^3, and Q^4 species, the line intensity depends, indeed, also on the type of the next-nearest neighbour species. This changes the coupling and the spatial extent of the vibration mode in such a point that it can sometimes be possible to distinguish different types of a given Q^n [58]. For Q^1 species, this argumentation is not relevant as they correspond to the upper end of modification of the silica network, and are then less coupled to the backbone. Q^1 Raman intensities will then be more precisely representative of the Q^1 population. Finally, the difference between the model and the Raman results can arise from the limitations of the SICA approach. First, the fact that we limit the cluster construction to the step $l=4$ does not permit to generate Q^0 as these species are made of a central tetrahedron that shares four Ca atoms (that structure would be created by $l=5$). As a consequence, the distribution of our Q^n ($n=4$, 3) are slightly

overestimated in the high calcium range. Second, as the energetical factors are introduced only on the basis of the overall mechanical character of the bonding type (stressed, isostatic, floppy) between two basic units, difficulties arise in order to describe the behaviour with changing alkaline earth cation as the size (or energetics, or steric hindrance, ...) does not appear in this approach. This means that other ingredients [44] are necessary to describe the differences arising in e.g. magnesium or barium silicates.

Next, we can focus on equilibrium constant [59] K_{c1} and K_{c2} between species respectively related to the equilibria:

$$Si_2O_5^{2-} \rightleftharpoons SiO_2 + SiO_3^{2-} \tag{11}$$

$$4SiO_3^{2-} \rightleftharpoons Si_2O_5^{2-} + Si_2O_7^{6-} \tag{12}$$

The mass action constants can be computed from the above equilibria using the computed distribution of Q^n species. It is obvious that equation (11) will be the dominant equation in the low calcium region while both equilibria will have to be taken into account in the concentration range lying around the rigid to floppy transition when NBO/T is larger than the value 1. As one can see from the insert of figure 9, the calculated K_{c1} from the equilibrium constant of (11) is in fair agreement with the two data points number reported by Frantz and Mysen [41]. We note also that K_{c1} remains almost constant over the entire concentration range of interest suggesting that the conversion between species is not favoured in the stressed rigid side of the glass formation range. On the other hand, the rapid variation of K_{c2} can arise from the floppy nature of the backbone, when $NBO/T > 1.25$. The change in equilibrium constant following the underlying elastic nature of the network has been questioned by Eckert and co-workers in phosphorus chalcogenides [60].

5.2. *Boolchand intermediate phase*

We now turn to self-organization that permits to obtain an elastic intermediate phase [23, 24]. This elastic phase has been first observed by Boolchand and co-workers in chalcogenides [34], but as rigid to floppy transitions have been also detected in oxide glasses [61], there is no reason why this intermediate phase should not exist in the present system as well. We consider here the structural possibilities that can lead to an intermediate phase. It is achieved with SICA by selecting the pathways of cluster production. One starts, for example, with an underconstrained (floppy) cluster of size l which exists at high calcium concentration. Agglomeration of basic units $l=1$ onto this cluster is only allowed if the creation of a stressed rigid region can be avoided on the generated cluster of size ($l=1$). This would happen if one starts to connect two $SiO_{4/2}$ tetrahedra together, involving an energy gain of E_s. On the other hand, if x is decreased one will accumulate with this rule isostatically rigid regions on the generated clusters as the only allowed concentrations are either floppy CaO–CaO or CaO–$SiO_{4/2}$ bondings. Alternatively, if one starts from the low calcium side, self-organization can be obtained by selecting along the same scheme stressed rigid and isostatically rigid connections and excluding systematically the possibility of floppy CaO–CaO bonding in the SICA construction.

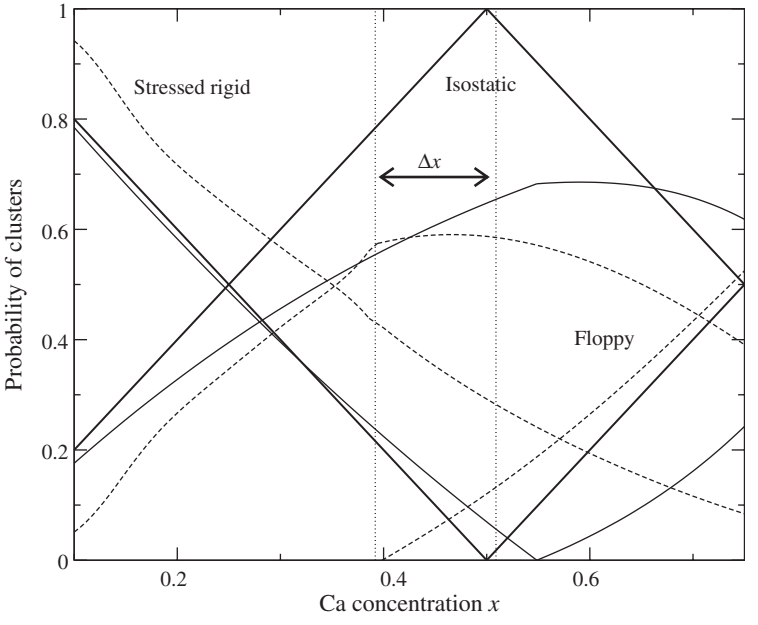

Figure 10. Probability of finding stressed rigid, isostatically rigid, and floppy clusters as a function of calcium concentration x. The thick solid line corresponds to the basic SICA step $l=1$ and $l=2$, the thin solid line to $l=3$, and the broken line to $l=4$. The vertical lines define the intermediate phase of width Δx at step $l=4$. The present situation for $l=3$ and $l=4$ corresponds to self-organization with ring structures. Notice the kink around $x=0.40$ corresponding to the stress transition (see text for details).

With decreasing calcium content, one will be able to maintain that rule up to a certain point beyond which connections between two silicon tetrahedra (or a stressed rigid connection) can not be avoided anymore. The latter point corresponds to a stress transition [24] and appears only if some medium range order (MRO) made of rings is accepted in the construction. The concentration range bounded on its low calcium side by the stress transition and on its high calcium side by the vanishing of the number of floppy modes, defines the intermediate phase of width Δx.

Results of self-organization are displayed in figure 10. The simplest case for self-organized clusters is again the case where rings are removed from the construction corresponding to dendritic clusters, which would correspond in the limit $l \to \infty$ to Bethe lattice solutions [62] or Random Bond models [63] obtained in the context of floppy to rigid transitions. We obtain here a single transition for all SICA steps l either at the mean-field value $x=x_c=0.50$ or close to it ($x_c=0.509(7)$ for $l=4$). No intermediate phase is obtained. The probabilities of floppy, isostatically rigid, and stressed rigid clusters can be displayed as a function of calcium content (figure 10) and show that the abundance of isostatically rigid clusters is maximum at the threshold defined by $f=0$. This is obviously the case for the $l=2$ case, but also for larger SICA steps.

The intermediate phase shows up if a certain amount of medium range order (MRO) is allowed. This is realized in the SICA construction by generating in the

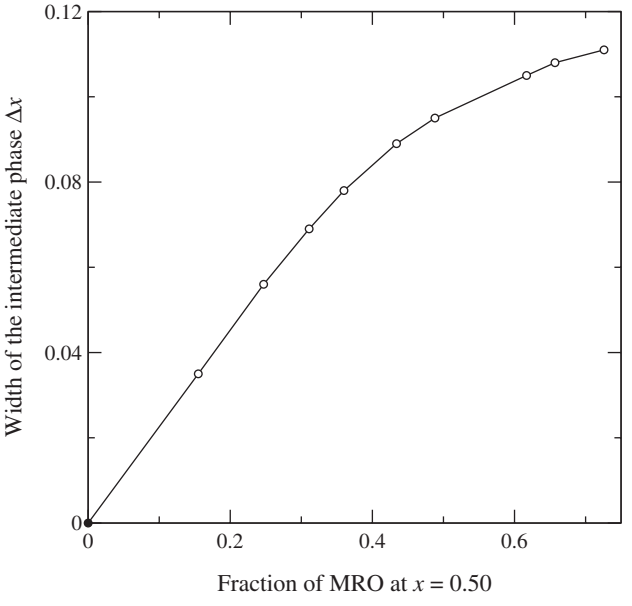

Figure 11. Width of the intermediate phase at step $l=4$ in $(1-x)SiO_2 - xCaO$ glasses, as a function of the fraction of medium range order (rings) computed at $x=0.50$. The insert represents the computed number of floppy modes for step $l=3$ (solid line) and $l=4$ (broken line).

construction ring clusters such as the one displayed in figure 7. The requirement of self-organization in the cluster construction still holds for dendritic stressed rigid structures made of at least two connected $SiO_{4/2}$ tetrahadra which propagate stress in the structure. But now cyclic structures such as rings are preserved from self-organization. Two transitions are obtained for every SICA steps $l > 2$ (see figure 10). The first transition lies always around the concentration $x_{c2}=0.50$ calcium and corresponds to a rigidity transition where the number of floppy modes vanishes. The second transition that emerges with increasing MRO is located for $l=4$ at $x_{c1}=0.392$ and corresponds to the stress transition. When starting from a floppy network at high calcium concentration, the progressive stiffening of the network can be accomplished by requirement of self-organization leading to the accumulation of isostatically rigid regions and stressed rigid ring structures. This will work for any decreasing x up to x_{c2} below which stressed rigid bondings outside of ring structures cannot be avoided anymore.

The two transitions x_{c1} an x_{c2} will define an intermediate phase Δx that depends on the fraction of MRO allowed and we show that Δx is an increasing function of the MRO (figure 11). Furthermore, as the rigidity transition $f=0$ at x_{c2} is almost not affected by the presence of MRO, the increase of the width with the latter quantity arises mostly from the decrease of x_{c1} with growing MRO. Finally, as seen from figure 10, there is a kink observable at x_{c1}, which would produce in first-order derivatives such as the energy [64], a jump suggesting a first-order stress transition at x_{c1} [23, 24] and a continuous rigidity transition at x_{c2}.

The elastic nature of the network can be also analyzed within this framework. From figure 10, one can see that the probability of finding isostatically rigid clusters is maximum in the window Δx. It is equal to 1 for the $l=2$ SICA step and about 0.5 or 0.6 for the larger steps, thus providing evidence that the molecular structure of the network in the window is almost stress-free.

6. Summary and Conclusions

We have shown in the present work from Raman measurements that a particular transition was observed at around 47% calcium in the calcium silicate system, in harmony with previous findings [13]. We have elucidated the origin of the observed threshold as being the manifestation of a global softening of the glass structure that corresponds to the manifestation of a rigid to floppy transition. Constraint-counting algorithms applied on size-increasing clusters permit to refine the picture by predicting the possibility of an intermediate phase in the Raman threshold region.

Recent calorimetric and spectroscopic studies have shown that this kind of elastic transitions could be found in alkaline silicates as well, with a well-defined signature of the intermediate phase in both sodium [31] and potassium glasses [65]. We are confident that a similar generic behaviour should be expected in the alkaline earth silicate glasses. An elegant probe for the existence of the intermediate phase in the present system could be given using MDSC measurements during the glass transition. The results present always a vanishing of the kinetic dependent heat flow inside that phase [34] and provide an unambiguous signature for both transitions, rigidity and stress. Unfortunately, the values of the glass transition temperatures of calcium silicates are too high to be accepted from the actual performances of the MDSC setup [66].

We finally emphasize the generic character of these rigid to floppy transitions that were originally found and extensively discussed in chalcogenides. Indeed, recent experiments and computer simulations now show that in oxide glasses these transitions can be produced either by chemical alloying like in the chalcogenides (or our present system) or with applied pressure [30].

Acknowledgements

The authors thank Emmanuel Veron for the EDX analysis and Boris Robert for help during the course of this work. LPTL is Unité Mixte de Recherche du CNRS n. 7600. CRMHT is Unité Propre du CNRS n. 4212.

References

[1] R. Gill (ed.), *Chemical Fundamentals of Geology* (Kluwer Academic, NY, 1996).
[2] J.F. Stebbins, P. McMillan and D. Dingwell (eds.), *Structure, Dynamics and Properties of Silicate Melts*, Review in Mineralogy, vol. 32, (Mineral. Soc. Am. Washington, D.C., 1995).
[3] F.A. Seifert, B.O. Mysen and D. Virgo, Geochim. Cosmochim. Acta **45** 1879 (1981).

[4] L. Gràsàsy, T. Wang and P.F. Jams, J. Chem. Phys. **108** 7317 (1998).
[5] V. Swamy and L.S. Dubrovinsky, Geochim. Cosmochim. Acta **61** 1181 (1997).
[6] J.B. Murdoch, J.F. Stebbins and I.S.E. Carmichaël, Am. Mineral. **70** 32 (1995).
[7] N.B. Basal and R.H. Doremus, *Handbook of Glass Properties* (Academic Press, New York, 1990).
[8] H. Doweidar, J. Non-Cryst. Solids **249** 194 (1999).
[9] S.S. Kim and T.H. Sanders Jr, J. Am. Ceram. Soc. **82** 1901 (1999).
[10] V.R. Mastelaro, E.D. Zanotto, N. Lequeux, *et al.*, J. Non-Cryst. Solids **262** 191 (2000).
[11] T. Taniguchi, M. Okuno and T. Matsumoto, J. Non-Cryst. Solids **211** 56 (1997).
[12] T. Taniguchi, M. Okuno and T. Matsumoto, Mineral. J. **17** 341 (1995).
[13] A.G. Kalampounias, G.N. Papatheodorou and S.N. Yannopoulos, J. Non-Cryst. Solids **322** 35 (2003).
[14] A.E. Geissberger and F.L. Galeener, Phys. Rev. B **28** 3266 (1983).
[15] W. Bresser, P. Boolchand and P. Suranyi, Phys. Rev. Lett. **56** 2493 (1986).
[16] R. Böhmer and C.A. Angell, Phys. Rev. B **45** 1091 (1992).
[17] J.C. Phillips, J. Non-Cryst. Solids **34** 153 (1979).
[18] M.F. Thorpe, J. Non-Cryst. Solids **57** 355 (1983).
[19] H. He and M.F. Thorpe, Phys. Rev. Lett. **54** 2107 (1985).
[20] A. Huerta and G.G. Naumis, Phys. Rev. Lett. **90** 145701 (2003); J. Non-Cryst. Solids **329** 100 (2003).
[21] W. Bresser, X. Feng and P. Boolchand, J. Non-Cryst. Solids **293–295** 348 (2001).
[22] T. Qu, D.G. Georgiev, P. Boolchand, *et al.*, Mater. Sci. Proc. **754** 111 (2003).
[23] M.F. Thorpe, D.J. Jacobs, M.V. Chubynsky, *et al.*, J. Non-Cryst. Solids **266–269** 859 (2000).
[24] M. Micoulaut and J.C. Phillips, Phys. Rev. B **67** 104204 (2003).
[25] F. Wang, S. Mamedov, P. Boolchand, *et al.*, Phys. Rev. B **71** 174201 (2005).
[26] S. Chakravarty, D.G. Georgiev, P. Boolchand, *et al.*, J. Phys. Cond. Matt. **17** L1 (2005).
[27] R. Monasson, R. Zecchina, S. Kirkpatrick, *et al.*, Nature **400** 133 (1999).
[28] J.C. Phillips, Phys. Rev. Lett. **88** 216401 (2002).
[29] A.J. Rader, B.M. Hespenheide, L.A. Kuhn, *et al.*, Proc. Natl. Acad. Sci. **99** 3540 (2002).
[30] K. Tachenko, M.T. Dove, V. Brazhkin, *et al.*, Phys. Rev. Lett. **93** 135502 (2004).
[31] Y. Vaills, T. Qu, M. Micoulaut, *et al.*, cond-mat/0406509.
[32] M. Malki, M. Micoulaut, F. Chaimbault, *et al.*, Europhys. Lett. **64** 661 (2003).
[33] P. Boolchand (ed.), *Insulating and Semiconducting Glasses* (World Scientific, Singapore, 2000).
[34] P. Boolchand, D.G. Georgiev and B. Goodman, J. OptoElec. Adv. Mater. **3** 703 (2001).
[35] J.E. Shelby, J. Appl. Phys. **50** 8010 (1979).
[36] O.V. Mazurin, M.V. Streltsina, T.P. Shvaiko-Shvaikovskaya, *Handbook of Glass Data*, Part A (Elsevier, Amsterdam, 1983).
[37] F.L. Galeener, A.J. Leadbetter and M.W. Stringfellow, Phys. Rev. B **27** 1052 (1983).
[38] R. Shuker and R.W. Gammon, Phys. Rev. Lett. **25** 222 (1970).
[39] D. De Sousa-Meneses, J.F. Brun, P. Echegut, *et al.*, Appl. Spectrosc. **58** 969 (2004).
[40] B. Hehlen, E. Courtens, A. Yamanaka, *et al.*, J. Non-Cryst. Solids **307–310** 87 (2002); B. Hehlen, E. Courtens, R. Vacher, *et al.*, Phys. Rev. Lett. **84** 5355 (2000).
[41] J.D. Frantz and B.O. Mysen, Chem. Geol. **121** 155 (1995).
[42] N. Zotov, J. Non-Cryst. Solids **287** 231 (2001).
[43] D. Selvenathan, W. Bresser and P. Boolchand, Phys. Rev. B **61** 15061 (2000).
[44] R. Kerner and J.C. Phillips, Solid State Comm. **117** 47 (2000).
[45] M. Zhang and P. Boolchand, Science **266** 1355 (1994).
[46] K. Trachenko, M.T. Dove, K.D. Hammonds, *et al.*, Phys. Rev. Lett. **81** 3431 (1998); K. Trachenko, M.T. Dove, M.J. Harris, *et al.*, J. Phys. Cond. Matt. **12** 8041 (2000).
[47] I. Farnan, P.J. Grandinetti, J.H. Baltisberger, *et al.*, Nature **358** 31 (1992).
[48] D.K. Belashenko, Inorg. Mater. **32** 160 (1996).
[49] A.G. Clare, A.C. Wright and R.N. Sinclair, J. Non-Cryst. Solids **213–214** 321 (1994). In this study is also found that there are two types of Na–O distances.
[50] X. Feng, W. Bresser and P. Boolchand, Phys. Rev. Lett. **78** 4422 (1997).

[51] R. Kerner, K. Penson and K.H. Bennemann, Europhys. Lett. **19** 363 (1992).
[52] R. Kerner and D.M. dos Santos-Loff, Phys. Rev. **B** 37 3881 (1988).
[53] M. Micoulaut, R. Kerner and D.M. dos Santos-Loff, J. Phys. Cond. Matt. **7** 8035 (1995).
[54] F.L. Galeener, D.B. Kerwin, A.J. Miller, *et al*., Phys. Rev. B **47** 7760 (1993).
[55] A.C. Wright, G. Etherington, J.A. Derwin-Desa, *et al*., J. Non-Cryst. Solids **49** 63 (1982).
[56] P.J. Bray, S.A. Feller, G.E. Jellison, *et al*., J. Non-Cryst. Solids **38**–**39** 93 (1980).
[57] K.S. Mills, ISIJ Intern. **33** 148 (1993).
[58] F. Chaimbault, PhD Thesis, University of Orléans (2004).
[59] B.O. Mysen, *Structure and Properties of Silicate Melts* (Elsevier, Amsterdam, 1988).
[60] R. Maxwell and H. Eckert, J. Am. Ceram. Soc. **116** 682 (1994); In $P_x - Se_{1-x}$ glasses, onset of rigidity appears for $x = 0.28$ phosphorus; See D.G. Georgiev, P. Boolchand, H. Eckert, M. Micoulaut and K.A. Jackson, Europhys. Lett. **62** 49 (2003).
[61] M. Zhang and P. Boolchand, Science **266** 1355 (1994).
[62] M.F. Thorpe, D.J. Jacobs and N.V. Chubynsky, *Rigidity Theory and Applications* (Kluwer Academic/Plenum Press, New York, 1999).
[63] D.J. Jacobs and M.F. Thorpe, Phys. Rev. Lett. **80** 5451 (1998).
[64] G.G. Naumis, Phys. Rev. B **62** R9205 (2000).
[65] F. Chaimbault, M. Micoulaut, Y. Vaills, *et al*., unpublished.
[66] http://www.tainst.com